Nucleation of superconductivity in clean superconductor-ferromagnet hybrid structures with Rashba spin-orbit interaction

A. A. Kopasov * and A. S. Mel'nikov
Institute for Physics of Microstructures, Russian Academy of Sciences, 603950 Nizhny Novgorod, GSP-105, Russia
and Lobachevsky State University of Nizhny Novgorod, 603950 Nizhny Novgorod, Russia

(Received 1 March 2022; revised 28 April 2022; accepted 31 May 2022; published 9 June 2022)

We study the influence of the inverse proximity effect on the nucleation of superconductivity in planar hybrid structures consisting of a thin superconducting film proximity coupled to a material with a strong exchange or Zeeman field and the Rashba spin-orbit interaction. Based on numerical simulations and analytical estimates within the framework of the Gor'kov equations, we find the superconducting transition temperature of the system and determine the spatial structure of the gap function. It is shown that the spin-orbit interaction partially compensates the pair-breaking effect of the exchange or Zeeman field and stabilizes modulated superconducting states, which can be traced to the Lifshitz invariant in the Ginzburg-Landau free-energy density. The suggested approach provides a microscopic justification of this invariant for a large class of superconducting hybrid systems and clarifies the validity range of the corresponding phenomenological models with terms linear in the spatial gradients of the superconducting order parameter.

DOI: 10.1103/PhysRevB.105.214508

I. INTRODUCTION

The influence of the spin-orbit interaction on the superconducting proximity effect in hybrid structures involving conventional superconductivity and strong exchange or Zeeman fields has been intensively studied in the past two decades. First, the spin-orbit coupling represents one of the key ingredients for engineering the topological superconductivity and realization of the Majorana zero modes [1–10]. Prominent examples of hybrid systems with predicted nontrivial topology of the superconducting condensate include proximized topological insulators [11–15] and semiconducting nanowires [16–22]. Second, the spin-orbit interaction also gives rise to a variety of novel phenomena in superconducting transport which can be used to expand the functionalities of the devices of superconducting spintronics [23,24]. In particular, it is responsible for the formation of Josephson φ_0 junctions with a spontaneous phase difference in the ground state [25–36], the appearance of spontaneous supercurrents [37–40], and the superconducting diode effect [26,28,31,33,41,42].

One of the central questions in the physics of the superconducting proximity effect is whether the coupling to the adjacent material can lead to the suppression of the parent superconductivity (the so-called inverse proximity effect). Existing theoretical studies point out that even for hybrid structures with highly transparent interfaces this effect can be vanishingly small if the normal-state electronic density of states at the Fermi level in the superconducting (S) layer is much larger than the one in the adjacent material [43]. Note that this reasoning does not include the effects of possible spin-dependent interactions in the adjacent layer. On the other hand, strong spin polarization in the adjacent layer can suppress the parent superconductivity even if the corresponding layer is an insulator [44–48]. The first theoretical description of this effect for superconductor/ferromagnetic insulator bilayers in the clean-limit regime was given by Tokuyasu *et al.* [44]. The origin of the pair-breaking effect stems from the fact that the quasiparticle wave functions acquire spin-dependent phase shifts upon the reflection from the spin-active interface (see also Ref. [23]). One can naturally expect that the spin-orbit interaction being taken into consideration should suppress the pair-breaking effect of the exchange or Zeeman field and enhance the superconducting transition temperature. Such an expectation is based on the results of theoretical works which have studied this effect in superconductors with an intrinsic or interfacial spin-orbit interaction (see, e.g., Refs. [49–51]). However, to the best of our knowledge, generalization of the approach used in Ref. [44] for superconducting proximity-coupled systems featuring both strong exchange or Zeeman field and the spin-orbit interaction in the adjacent material is absent in the literature. Our work addresses this question and provides such a generalization. Note that an analysis of the influence of spin-dependent scattering phase shifts on the inverse proximity effect is beyond the range of validity of the tunneling Hamiltonian approach which was previously used to analyze this effect in hybrid systems with a nontrivial topology [52–56]. In this regard, the analysis of the scattering phase shifts can be important for establishing the role of the inverse proximity effect in proximized semiconducting nanowires and topological insulators which a number of recent experiments [57–59] claimed to observe.

It is remarkable that the vast majority of the physical phenomena arising due to the interplay of superconductivity, spin-splitting fields, and the spin-orbit interaction can be described phenomenologically within the framework of

*Corresponding author: kopasov@ipmras.ru

the modified Ginzburg-Landau (GL) theory with the term linear in the gradient of the superconducting order parameter $\sim(\mathbf{n}\times\mathbf{n}_h)(\nabla\Delta)\Delta^*$ (the so-called Lifshitz invariant) [25,37–41]. Here $\nabla=(\partial_x,\partial_y,\partial_z)$, $\mathbf{n}$ ($\mathbf{n}_h$) is the unit vector along the axis with broken inversion (spin rotation) symmetry, and Δ is the superconducting order parameter. The development of a microscopic description of the inverse proximity effect is of particular importance since it should justify the appearance of the Lifshitz invariant in commonly used phenomenological models and should also clarify their validity range. Although the GL functional was derived from a microscopic theory for superconductors with the intrinsic spin-orbit interaction in both the clean and diffusive limits [60–66], justification of the Lifshitz invariant in proximity-coupled systems is an unsettled problem. Note that a similar problem arises for superconducting hybrid structures in which the adjacent layer possesses a textured magnetization. In particular, the GL free energy of a conventional superconductor coupled to a helimagnet was microscopically derived in Ref. [67].

In this paper, we study the influence of the inverse proximity effect on the nucleation of superconductivity in three-dimensional superconductor-ferromagnet hybrid structures with Rashba spin-orbit interaction. Using the exact normal-state solutions of the Gor'kov equations, we derive the linearized self-consistency equation and determine the superconducting transition temperature of the system and the spatial structure of the gap function. The suggested microscopic approach addresses the clean-limit regime and takes into account the effects of strong hybridization between quasiparticle states in both layers. It is shown that the spin-orbit coupling partially compensates the pair-breaking effect of the exchange field and stabilizes modulated superconducting states with a finite center-of-mass Cooper pair momentum which can be traced to the Lifshitz invariant in the GL free-energy density. We demonstrate the tunability of the resulting pair momentum as a function of the chemical potential in the adjacent material and the reentrant behavior of the pair momentum versus the spin-splitting field and the energy of the spin-orbit interaction. All the spin-dependent effects under consideration are explained using qualitative band structure analysis, and an approximate analytical expression governing the behavior of the critical temperature with respect to the energy of the spin-orbit interaction is given.

It is important to note that the validity of our results is restricted to the case when the density of states at the Fermi level in the normal-metal state of the S layer is much larger than the one in the adjacent material. Nevertheless, our results are applicable for a large class of hybrid structures with the spin-orbit interaction, including superconductor/semiconductor, superconductor/ferromagnetic metal (insulator), and superconductor/completely spin-polarized metal (the so-called half metal [68,69]) hybrids. Superconductor/half-metal systems are of special interest for superconducting spintronics. The full spin polarization for the electrons in half metals makes such hybrid systems a convenient platform to study the long-range triplet Josephson transport [70,71] and the triplet spin-valve effect [72,73].

Our results for the spin-orbit-enhanced superconducting critical temperature and the behavior of the spontaneous Cooper pair momentum qualitatively agree with the results of recent works which have considered similar effects in three-dimensional diffusive [74] and two-dimensional ballistic [75] superconductor-ferromagnet heterostructures as well as in superconductor-ferromagnet bilayers on top of a topological insulator [76].

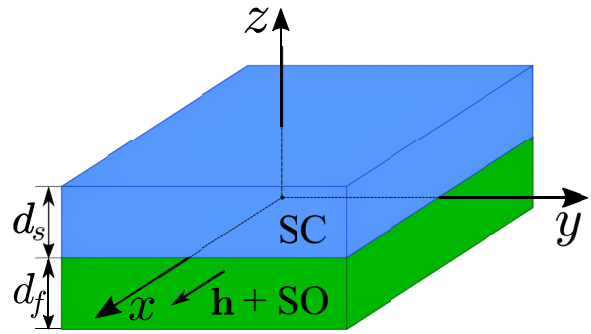

FIG. 1. Schematic picture of the superconducting film placed in contact with a material with the exchange or Zeeman field $\mathbf{h}$ and the Rashba spin-orbit interaction with a unit vector $\mathbf{n}$ aligned along the z axis (not shown). Here d_s (d_f) is the thickness of the superconducting (adjacent) layer.

This paper is organized as follows. In Sec. II we introduce the model and basic equations. In Sec. III we present linearized self-consistency equations and explain how the suggested microscopic approach can be used to deduce the structure of the relevant phenomenological description. In Sec. IV we provide qualitative arguments regarding the joint effect of the exchange field and the spin-orbit interaction on the superconducting critical temperature and the spatial structure of the gap function. In Sec. V the results of numerical simulations are presented and discussed. Finally, the results are summarized in Sec. VI.

II. BASIC EQUATIONS

Hereafter, we consider planar hybrid structures consisting of a thin superconducting film placed in contact with a material with a strong exchange or Zeeman field and the Rashba spin-orbit interaction (see Fig. 1). We assume that the conditions of the clean-limit regime are fulfilled in both layers. In the present work we consider the case $\lambda_F\ll d_s\ll\xi_s$, where d_s is the thickness of the S layer, λ_F is the Fermi wavelength in the normal-metal state of a superconductor, and ξ_s is the zero-temperature superconducting coherence length. The condition $d_s\ll\xi_s$ allows us to neglect spatial variations of the gap function over the thickness of the S layer. On the other hand, the condition $\lambda_F\ll d_s$ ensures that the effects associated with the size quantization of the quasiparticle energy spectrum in the superconducting film (see, e.g., Refs. [77–79]) are vanishingly small. Our focus is on the back-action of spin-dependent interactions in the adjacent layer on the superconducting critical temperature of the system [80]. Thus, we neglect the intrinsic paramagnetic effect for the electrons in the S layer and the orbital effects in both layers. Hereafter we use the units $k_B=\hbar=1$, where k_B is the Boltzmann constant and $\hbar$ is the Planck constant. The Hamiltonian of the system

reads

$$\hat{\mathcal{H}} = \sum_{\sigma\sigma'} \int d^3\mathbf{r}\ \psi^\dagger_\sigma(\mathbf{r})[\hat{H}(\mathbf{r})]_{\sigma\sigma'}\psi_{\sigma'}(\mathbf{r}) + \int d^3\mathbf{r}[\Delta(\mathbf{r})\psi^\dagger_\uparrow(\mathbf{r})\psi^\dagger_\downarrow(\mathbf{r}) + \Delta^*(\mathbf{r})\psi_\downarrow(\mathbf{r})\psi_\uparrow(\mathbf{r})]. \quad (1)$$

Here $\psi^\dagger_\sigma$ (ψ_σ) is the electron creation (annihilation) operator, the indices $\sigma, \sigma' = \uparrow, \downarrow$ denote spin degrees of freedom,

$$[\hat{H}(\mathbf{r})]_{\sigma\sigma'} = H_0(\mathbf{r})\delta_{\sigma\sigma'} + [\hat{U}(\mathbf{r})]_{\sigma\sigma'}, \quad (2a)$$

$$H_0(\mathbf{r}) = \mathbf{p}\frac{1}{m(\mathbf{r})}\mathbf{p} - \mu(\mathbf{r}) + U_0\delta(z), \quad (2b)$$

$\mathbf{p} = -i\nabla = (p_x, p_y, p_z)$ is the momentum operator, $m(\mathbf{r})$ is the spatially varying effective mass, $\mu(\mathbf{r})$ is the chemical potential profile, and the parameter $U_0 > 0$ describes an additional spin-independent potential barrier for quasiparticles at the interface. The spin-dependent potential $\hat{U}(\mathbf{r})$ is nonzero only in the adjacent layer,

$$\hat{U}(\mathbf{r}) = \Theta(-z)[h\hat{\sigma}_x + \alpha(p_x\hat{\sigma}_y - p_y\hat{\sigma}_x)], \quad (3)$$

where Θ denotes the Heaviside function, $\hat{\sigma}_i$ ($i = x, y, z$) are the Pauli matrices acting in the spin space, h is the exchange (or Zeeman) field, and α is the spin-orbit constant. The superconducting order parameter $\Delta(\mathbf{r})$ is nonzero only in the S layer ($0 \leqslant z \leqslant d_s$). Throughout this paper we use the following profile of the gap function (see the corresponding discussion in Sec. I):

$$\Delta(\mathbf{r}) = |\Delta|e^{iq(\mathbf{n}\times\mathbf{n}_h)\mathbf{r}}. \quad (4)$$

In the above expression $q(\mathbf{n}\times\mathbf{n}_h)$ is the center-of-mass Cooper pair momentum in the direction given by the cross product of the Rashba vector $\mathbf{n}$ and the unit vector $\mathbf{n}_h = \mathbf{h}/|\mathbf{h}|$ (see Fig. 1).

Our analysis is based on the Gor'kov equations for the Matsubara Green's functions. In the Matsubara frequency-coordinate representation they read

$$\check{G}^{-1}(\mathbf{r})\check{G}(\mathbf{r},\mathbf{r}') = \delta(\mathbf{r}-\mathbf{r}'), \quad (5a)$$

$$\check{G}^{-1}(\mathbf{r}) = \begin{bmatrix} i\omega_n - \hat{H}(\mathbf{r}) & \Delta(\mathbf{r}) \\ \Delta^*(\mathbf{r}) & i\omega_n + \hat{\sigma}_y\hat{H}^*(\mathbf{r})\hat{\sigma}_y \end{bmatrix}. \quad (5b)$$

Here $\omega_n = 2\pi T(n+1/2)$ is the Matsubara frequency, T is temperature, and n is an integer. The 4×4 matrix $\check{G}(\mathbf{r},\mathbf{r}')$ has the following block structure:

$$\check{G}(\mathbf{r},\mathbf{r}') = \begin{bmatrix} \hat{G}(\mathbf{r},\mathbf{r}') & \hat{F}(\mathbf{r},\mathbf{r}') \\ \hat{F}^\dagger(\mathbf{r},\mathbf{r}') & \hat{\bar{G}}(\mathbf{r},\mathbf{r}') \end{bmatrix}, \quad (6)$$

and the pairing potential is determined from the self-consistency equation

$$\Delta^*(\mathbf{r}) = \frac{VT}{2}\sum_{|\omega_n|<\Omega} \mathrm{Tr}[\hat{F}^\dagger(\mathbf{r},\mathbf{r})], \quad (7)$$

where V denotes the strength of the effective electron-electron interaction and Ω is the BCS cutoff frequency.

For the derivation of the linearized self-consistency equation we perform the perturbation expansion of Eqs. (5) with respect to the superconducting order parameter using stepwise profiles for the chemical potential and the effective mass. In the following section we present and discuss our analytical results, and the details of the derivation are given in the Supplemental Material [81].

III. LINEARIZED SELF-CONSISTENCY EQUATION

In the case of a homogeneous pair potential the linearized self-consistency equation reads

$$\ln\left(\frac{T}{T_{c0}}\right) = \pi T\sum_{\omega_n>0}\left[-\frac{2}{\omega_n} + \mathrm{Re}\sum_{\eta,\eta'=\pm}\left\langle\frac{\delta_{\eta\eta'}w_{\mathrm{intra}} + (1-\delta_{\eta\eta'})w_{\mathrm{inter}}}{\omega_n + i\rho_{\eta\eta'}}\right\rangle_{\mathbf{k}}\right]. \quad (8)$$

Here T_{c0} is the critical temperature of the bulk superconductor, η and η' are the indices of the spin-split helical subbands, $\langle\cdots\rangle_{\mathbf{k}}$ denotes the averaging over the Fermi surface of the S layer in the normal-metal state,

$$\langle X(\mathbf{k})\rangle_{\mathbf{k}} = \frac{1}{4\pi}\int_{-1}^{1} du \int_0^{2\pi} d\varphi\ X(\mathbf{k}), \quad (9)$$

$\mathbf{k} = (k_{||}\cos\varphi, k_{||}\sin\varphi, k_F u)$, $k_{||} = k_F\sqrt{1-u^2}$, and k_F (v_F) is the Fermi momentum (velocity) in the normal-metal state of a superconductor. The depairing factors

$$\rho_{\eta\eta'} = \frac{v_F}{2d_s}u\tan(\bar{\phi}_\eta - \phi_{\eta'}) \quad (10)$$

describe the suppression of the interband (ρ_{+-}, ρ_{-+}) and intraband (ρ_{++}, ρ_{--}) spin-singlet superconducting correlations in the S layer [82]. The effects of hybridization between electronic states in both layers are described by the scattering phase shifts

$$\tan(\phi_\eta) = \frac{1}{Z + (m_s k_{f\eta}/m_f k_s)\cot(k_{f\eta}d_f)}, \quad (11)$$

which contain the information about the spectral properties of both layers,

$$\frac{k^2_{f\eta}}{2m_f} = i\omega_n + \mu_{f\perp} - \eta\sqrt{(h-\alpha k_y)^2 + (\alpha k_x)^2}, \quad (12a)$$

$$\frac{k_s^2}{2m_s} = i\omega_n + \mu_{s\perp}, \quad (12b)$$

and the spatial extent of the electronic wave function inside the ferromagnet. Here μ_s and m_s (μ_f and m_f) are the chemical potential and the effective mass in the superconductor (ferromagnet), respectively, $\mu_{s(f)\perp} = \mu_{s(f)} - \mathbf{k}^2_{||}/2m_{s(f)}$, and $Z = 2m_sU_0/k_s$ is the barrier strength parameter. The scattering

phase shifts for holes $\bar{\phi}_\eta$ are obtained from Eq. (11),

$$\bar{\phi}_\eta(\omega_n, h) = \phi_\eta(-\omega_n, -h). \tag{13}$$

The weighting functions

$$w_{\text{inter}} = \cos^2(\beta), \tag{14a}$$

$$w_{\text{intra}} = 1 - w_{\text{intra}}, \tag{14b}$$

with $\beta = (\beta_+ + \beta_-)/2$ and $\tan(\beta_\pm) = \alpha k_x/(h \pm \alpha k_y)$, determine the distribution for the fraction of the spin-singlet interband (intraband) Cooper pairs on the Fermi surface.

To compare our results with the ones in Ref. [44], one should exclude from consideration the spin-orbit coupling and frequency dependences of the scattering phases, which results in the following relations:

$$w_{\text{inter}} = 1, \tag{15a}$$

$$\rho_{+-} = -\rho_{-+}. \tag{15b}$$

Using Eqs. (15), the self-consistency equation (8) can be written in the form

$$\ln\left(\frac{T}{T_{c0}}\right) = -\pi T \sum_{\omega_n} \int_0^1 du \frac{\rho^2(u)}{|\omega_n|\left[\omega_n^2 + \rho^2(u)\right]}, \tag{16a}$$

$$\rho(u) = \frac{v_F}{2d_s} u \tan\left[\phi_+(u) - \phi_-(u)\right], \tag{16b}$$

which is Eq. (33) in Ref. [44].

For a nonuniform profile of the gap function (4) with $q \neq 0$ the resulting self-consistency equation has the form (8) with the replacements

$$\bar{\phi}_\eta(k_x, k_y) \to \bar{\phi}_\eta(k_x, k_y - q/2), \tag{17a}$$

$$\phi_\eta(k_x, k_y) \to \phi_\eta(k_x, k_y + q/2), \tag{17b}$$

$$\beta_+(k_x, k_y) \to \beta_+(k_x, k_y - q/2), \tag{17c}$$

$$\beta_-(k_x, k_y) \to \beta_-(k_x, k_y + q/2) \tag{17d}$$

and modified depairing factors

$$\rho_{\eta\eta'}(q) = \frac{q v_F}{2} \sin(\varphi)\sqrt{1-u^2} + \frac{v_F}{2d_s} u \tan[\bar{\phi}_\eta(q) - \phi_{\eta'}(q)]. \tag{18}$$

In the presence of the spin-splitting field and the spin-orbit coupling we determine both the superconducting transition temperature

$$T_c = \max_q \left[T_c(q)\right] \tag{19}$$

and the Cooper pair momentum $q = Q$ corresponding to a maximal T_c.

The analysis of the resulting $Q(\alpha, h)$ dependences provides important information about the structure of the relevant phenomenological description. In particular, such an analysis can be used to justify the appearance of the Lifshitz invariant in the GL free-energy density and can reveal the validity range of such a description. The idea is as follows [83]. Substituting the order parameter profile (4) into the free-energy density with the Lifshitz invariant

$$f(\mathbf{r}) = -a(\tilde{T}_c - T)|\Delta|^2 + \frac{\beta}{2}|\Delta|^4 + \gamma|\mathbf{p}\Delta|^2 + \epsilon(\mathbf{n} \times \mathbf{n}_h)[\Delta^*(\mathbf{p}\Delta) + \text{c.c.}], \tag{20}$$

we get the free energy without the Lifshitz invariant but with shifted critical temperature

$$T_c(q) = \tilde{T}_c - \frac{\gamma}{a}\left(q + \frac{\epsilon}{\gamma}\right)^2 + \frac{\epsilon^2}{a\gamma}. \tag{21}$$

Here a, β, and γ are the standard GL coefficients, and $\tilde{T}_c = T_c(q = 0)$. The resulting pair momentum Q determines the value of the Lifshitz invariant, and the shift in T_c is quadratic in Q,

$$\epsilon = -\gamma Q, \tag{22a}$$

$$\delta T_c(Q) \equiv T_c(Q) - T_c(0) = \frac{\gamma}{a} Q^2. \tag{22b}$$

Deviations of the resulting $\delta T_c(Q)$ behavior obtained from a microscopic model from the one given in Eq. (22b) signal the breakdown of the initial assumption (20), and thus, the terms involving higher-order spatial gradients have to be included in the phenomenological theory for the correct description of the inverse proximity effect.

IV. CRITICAL TEMPERATURE AND THE PAIR MOMENTUM: QUALITATIVE CONSIDERATION

Here we provide qualitative arguments regarding the joint effect of the spin-splitting field and the spin-orbit interaction on the superconducting critical temperature and the emerging pair momentum. A lot of insights can be gained from the fact that under the conditions of the inverse proximity effect both the exchange field and the spin-orbit coupling are induced in the S layer. Schematic plots of the Fermi surfaces for two-dimensional spin-split subbands confined in the direction perpendicular to the plane of the layers are shown in Fig. 2.

For simplicity, we discuss the behavior of T_c for a homogeneous gap function. Figure 2(a) illustrates that in the absence of the spin-orbit coupling the spin-singlet Cooper pairs are formed by the electrons from different spin-split subbands. This regime corresponds to $w_{\text{inter}} = 1$ in Eq. (8). The spin dependence of the scattering phase shifts results in a rather strong suppression of T_c upon the increase in h which is accompanied by the appearance of the odd-frequency spin-triplet superconducting correlations in the S layer with zero spin projection in the direction of the exchange or Zeeman field [23]. On the contrary, for $h = 0$, $\alpha \neq 0$ there is only the intraband spin-singlet pairing in the S layer [see Fig. 2(c)], and the corresponding scattering phase shifts are spin independent. In this case, the spin-orbit coupling results in an increase in the density of states at the Fermi level in the adjacent material due to the increase in μ_f by the amount $m_f\alpha^2$. In a typical experimental situation $m_f\alpha^2 \ll \mu_s$, and the separate effect of the spin-orbit interaction on T_c should be negligibly small.

For finite h and α there are both intraband and interband spin-singlet Cooper pairs in the S layer, and their overall fractions on the Fermi surface

$$W_{\text{inter}} = \langle w_{\text{inter}} \rangle_{\mathbf{k}}, \tag{23a}$$

$$W_{\text{intra}} = 1 - W_{\text{inter}} \tag{23b}$$

are determined by the ratio $h/\alpha k_F$. Thus, in the limit $h \gg \alpha k_F$ ($h \ll \alpha k_F$) the interband (intraband) pairing dominates in the

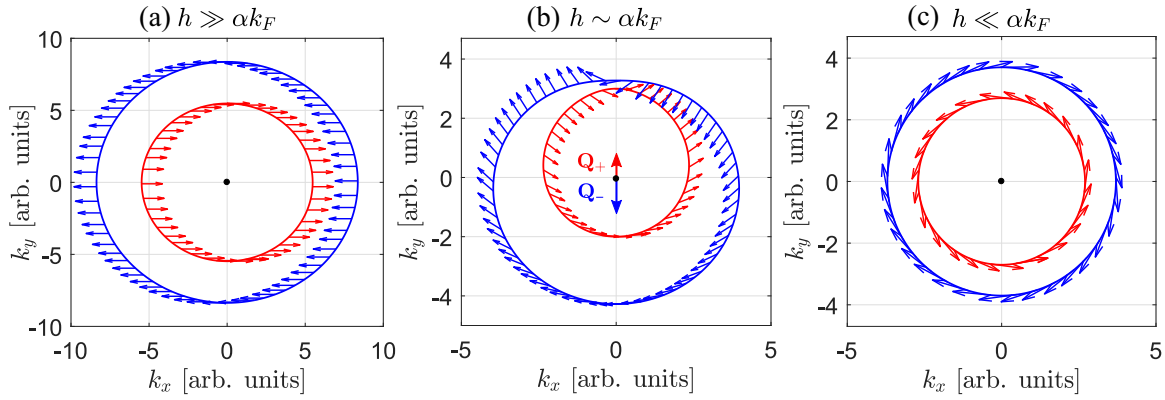

FIG. 2. Schematic plots of the normal-state two-dimensional Fermi surfaces for spin-split subbands confined in the direction perpendicular to the plane of the layers. (a)–(c) correspond to the limits $h \gg \alpha k_F$, $h \sim \alpha k_F$, and $h \ll \alpha k_F$, respectively, and arrows show the spin polarization. Here k_F is the Fermi momentum in the normal-metal state of a superconductor. Vectors $\mathbf{Q}_\eta$, with $\eta = \pm$, in (b) highlight the difference in the Cooper pair momenta within each spin-split subband.

system. Qualitative analysis of Eqs. (10), (11), (12a), and (13) shows that the exchange field suppresses both the intraband and interband spin-singlet superconducting correlations and such suppression is stronger for the interband Cooper pairs. This particular observation allows us to expect that the spin-orbit interaction should partially compensate the effect of the exchange field $T_c(\alpha k_F \gg h, h) \geqslant T_c(\alpha = 0, h)$. Rather simple formulas describing $T_c(\alpha k_F, h)$ behavior can be derived from Eq. (8) by decoupling the Fermi surface averages,

$$\left\langle \frac{w_{\text{intra}}}{\omega_n + i\rho_{\eta\eta}} \right\rangle_{\mathbf{k}} \approx W_{\text{intra}} \left\langle \frac{1}{\omega_n + i\rho_{\eta\eta}} \right\rangle_{\mathbf{k}}, \tag{24a}$$

$$\left\langle \frac{w_{\text{inter}}}{\omega_n + i\rho_{\eta\bar{\eta}}} \right\rangle_{\mathbf{k}} \approx W_{\text{inter}} \left\langle \frac{1}{\omega_n + i\rho_{\eta\bar{\eta}}} \right\rangle_{\mathbf{k}}, \tag{24b}$$

and neglecting the spin-orbit coupling in the scattering phase shifts as αk_F varies from zero to $\alpha k_F \gg h$. Here $\bar{\eta} = -\eta$. As a result, we get the following expression:

$$\frac{T_c(\alpha k_F, h)}{T_{c0}} = \left[\frac{T_c(\alpha = 0, h)}{T_{c0}}\right]^{W_{\text{inter}}} \left[\frac{T_c(\alpha k_F \gg h, h)}{T_{c0}}\right]^{W_{\text{intra}}}, \tag{25}$$

which is in good qualitative agreement with the results of our numerical simulations.

Let us now discuss the behavior of the center-of-mass Cooper pair momentum near the superconducting critical temperature with respect to the band structure parameters of the adjacent material. In our qualitative considerations we address only the intraband pairing assuming that the interband superconducting correlations should affect the spatial structure of the gap function at much lower temperatures. First, one can see from Fig. 2(b) that for $h \sim \alpha k_F$ each helical subband with $\eta = \pm$ favors an inhomogeneous superconducting state with a finite Cooper pair momentum $\mathbf{Q}_\eta$ in the opposite directions $\eta(\mathbf{n} \times \mathbf{n}_h)$. The resulting pair momentum originates from the competition between two helical subbands, and their difference in the densities of states in the normal-metal state of the S layer at the Fermi level is crucial in order to obtain a nonvanishing result [66]. In particular, this implies that for fixed h and αk_F the pair momentum should be highly sensitive to the value of the chemical potential in the adjacent layer μ_f. Second, the transformations $h \to -h$ and $\alpha \to -\alpha$ correspond to $k_y \to -k_y$ in Fig. 2, from which we get the following symmetry relations:

$$Q(\alpha, h) = -Q(-\alpha, h), \tag{26a}$$

$$Q(\alpha, h) = -Q(\alpha, -h). \tag{26b}$$

Third, Figs. 2(a) and 2(c) demonstrate that the pair momentum Q vanishes in the limits $h \gg \alpha k_F$ and $h \ll \alpha k_F$. Therefore, one can expect reentrant $Q(h)$ and $Q(\alpha k_F)$ dependences with max $|Q|$ at $h \sim \alpha k_F$.

V. RESULTS AND DISCUSSION

We proceed to the discussion of the results of numerical simulations. The appearance of the spin-dependent effects under consideration is illustrated for $m_f/m_s = 1$ and $U_0 = 0$. The effects of the adjacent layer on the superconducting critical temperature obviously diminish with the increase in the thickness of the superconducting film and/or with the decrease in the coupling strength. The latter can be provided by introducing strong spin-independent scattering at the material interface and/or large effective mass mismatch.

Typical behavior of the superconducting critical temperature with respect to the spin-dependent fields in the adjacent layer is shown in Fig. 3. The parameters are $\mu_s/T_{c0} = 10^4$, $\mu_f = 0$, $d_s T_{c0}/v_F = 0.01$, and $d_f = 5d_s$. Note that for the chosen μ_f the results for weak ($h \leqslant T_{c0}$) and strong ($h \gg T_{c0}$) spin-splitting fields refer to superconductor/semiconductor and superconductor/half-metal heterostructures, respectively. Several $T_c(\alpha k_F)$ plots for different spin-splitting fields h are shown in Fig. 3(a). One can see that in the absence of the exchange field the spin-orbit coupling has almost no effect on the superconducting critical temperature. Increasing h from zero results in a rather strong suppression of T_c which is partially compensated by the spin-orbit coupling. Thin solid lines in Fig. 3(a) show the results of Eq. (25). Typical $T_c(h)$ plots for several energies of the spin-orbit coupling shown in Fig. 3(b) reveal the decrease in the slopes of $T_c(h)$ dependences upon the increase in αk_F. As explained in the previous

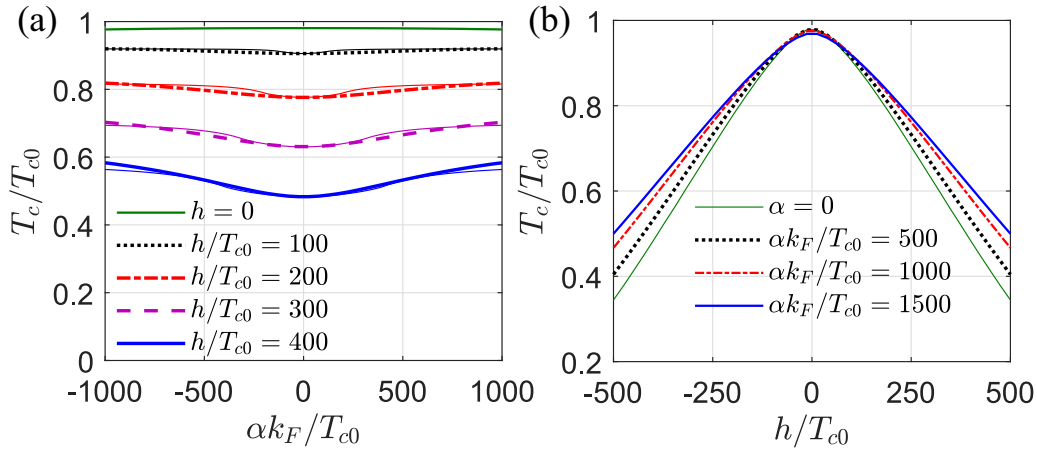

FIG. 3. (a) Superconducting critical temperature T_c versus the energy of the spin-orbit coupling αk_F for $h/T_{c0} = 0$, 100, 200, 300, 400. Thin solid lines show the results of Eq. (25). (b) $T_c(h)$ plots for $\alpha k_F/T_{c0} = 0$, 500, 1000, 1500. The parameters are $\mu_s/T_{c0} = 10^4$, $\mu_f = 0$, $d_s T_{c0}/v_F = 0.01$, and $d_f = 5d_s$. Here v_F is the Fermi velocity in the normal-metal state of a superconductor, and T_{c0} denotes the critical temperature of the bulk superconductor.

section, such a compensation effect originates from the appearance of the intraband spin-singlet pairing correlations in the superconducting layer for which the depairing effect of the exchange field is weaker. For both Figs. 3(a) and 3(b) we find that $|Q|v_F/2T_{c0} < 0.05$ and the shift in T_c for a modulated superconducting state $\delta T_c(Q)/T_{c0} < 10^{-3}$.

Let us now briefly discuss the opposite case $\mathbf{h} = h_z\hat{\sigma}_z$ ($\mathbf{n}_h||\mathbf{n}$). It can be shown that the equation for T_c has the form (8) with the weighting function

$$w_{\text{intra}}(\mathbf{k}_{||}) = \alpha^2 k_{||}^2/\left(h_z^2 + \alpha^2 k_{||}^2\right) \tag{27}$$

and modified scattering phases due to a different spatial dispersion of the quasiparticle states in the ferromagnet

$$k_{f\eta}^2 = 2m_f\left(i\omega_n + \mu_{f\perp} - \eta\sqrt{h_z^2 + \alpha^2 k_{||}^2}\right). \tag{28}$$

We observe that the behavior of T_c in the regime $\mathbf{n}_n||\mathbf{n}$ qualitatively agrees with the above-described case $\mathbf{n}_h \perp \mathbf{n}$. However, the compensation effect of the spin-orbit coupling is more significant for the out-of-plane exchange field $\mathbf{n}_h||\mathbf{n}$. This quantitative difference originates from the fact that the depairing factors $\rho_{\eta\eta}$ ($\eta = \pm$) which determine the pair-breaking effect of the exchange field for the intraband Cooper pairs and the resulting enhancement of the critical temperature appear to be sensitive to the relative orientation between $\mathbf{n}_h$ and $\mathbf{n}$. Qualitative analysis of Eqs. (10), (11), (12a), (13), and (28) reveals that $\rho_{\eta\eta}$ are generally lower for the out-of-plane exchange field than for the in-plane one. We provide a comparison between our numerical simulations for both system configurations $\mathbf{n}_h \,||\, \mathbf{n}$ and $\mathbf{n}_h \perp \mathbf{n}$ in the Supplemental Material [81].

Before we proceed further, let us note that our qualitative arguments regarding the behavior of T_c are also valid for thin superconducting films under the influence of a strong Zeeman field and the induced spin-orbit coupling. In this regard, our results also clarify the quench of the paramagnetic effect for the electrons in thin superconducting films coupled to heavy metals with a strong spin-orbit interaction. Note that this effect was analyzed in the context of the superconducting proximity effect in semiconductor-superconductor hybrids in a recent experiment [84] in which it was demonstrated that InSb nanowires strongly coupled to Al/Pt films can maintain superconductivity up to 7 T.

We continue with a discussion of the behavior of the center-of-mass Cooper pair momentum. The resulting pair momentum Q, indeed, appears to be highly sensitive to the chemical potential in the adjacent material. Typical $Q(\mu_f)$ dependences for several h are shown in Fig. 4(a). We use the following parameters to produce the plots in Fig. 4: $\mu_s/T_{c0} = 10^3$, $d_s T_{c0}/v_F = 0.05$, $d_f = 4d_s$, and $\alpha k_F/T_{c0} = 200$. The parameter regime $|\mu_f| < h$ refers to the superconductor/half-metal heterostructures, and $\mu_f < -h$ ($\mu_f > h$) corresponds to the superconductor/ferromagnetic insulator (superconductor/ferromagnetic metal) hybrids. We can see that for a fixed exchange splitting the resulting $Q(\mu_f)$ curves are nonmonotonic and $|Q|$ is maximal when the lower spin-split subband in the ferromagnet crosses the Fermi level and the bottom of the higher spin-split subband is above the Fermi level. Such behavior reflects the competition between the spin-split helical subbands which favor modulated superconducting states with finite Cooper pair momenta of different magnitudes and in opposite directions. As mentioned in Sec. IV, a nonzero difference in the spin-resolved density of states in the normal-metal state of the S layer at the Fermi level $\nu_{s\eta}$ ($\eta = \pm$) is required in order to obtain a nonvanishing result. Using the approach developed in the present work, we can show that this difference is proportional to the Fermi surface average of the following quantity:

$$|\delta\nu_s| \equiv |\nu_{s+} - \nu_{s-}| \propto \left\langle \frac{\sin(2\phi_+) - \sin(2\phi_-)}{k_z d_s} \right\rangle_{\mathbf{k}}. \tag{29}$$

Typical behavior of $|\nu_{s+} - \nu_{s-}|$ with respect to μ_f is shown in Fig. 4(b). We can clearly see that nonmonotonic $|\delta\nu_s(\mu_f)|$ curves tracing the features in the density of states in the ferromagnet provide a qualitative explanation for the nonmonotonic $Q(\mu_f)$ behavior shown in Fig. 4(a).

The behavior of the pair momentum with respect to the spin-splitting field in the adjacent layer is shown in Fig. 5(a). We use the following parameter set to produce the results in

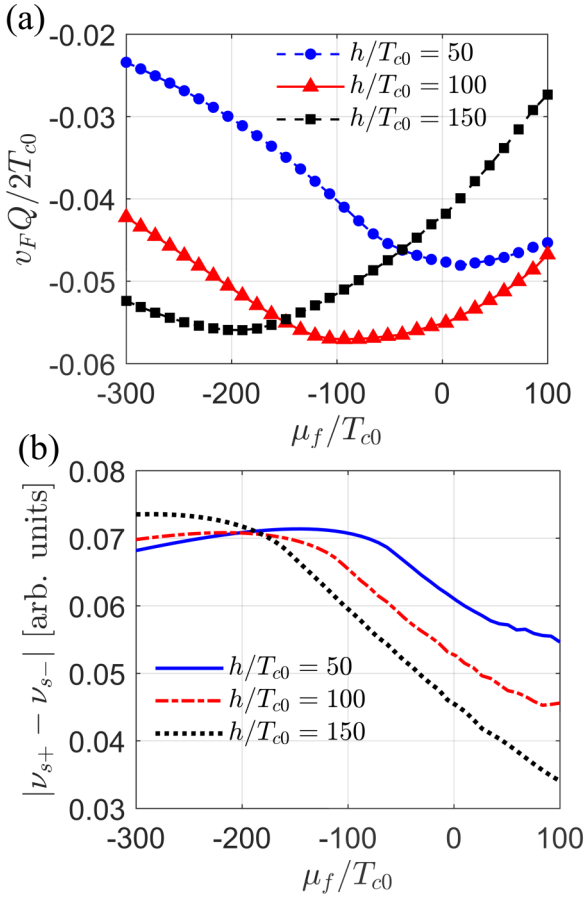

FIG. 4. (a) The Cooper pair momentum Q versus the chemical potential in the adjacent layer μ_f for several spin-splitting fields $h/T_{c0} = 50, 100, 150$. (b) Absolute value of the difference between the spin-resolved densities of states in the normal-metal state of the S layer at the Fermi level $\nu_{s\eta}$ ($\eta = \pm$) versus μ_f for $h/T_{c0} = 50, 100, 150$. The parameters are $\mu_s/T_{c0} = 10^3$, $d_s T_{c0}/v_F = 0.05$, $d_f = 4d_s$, and $\alpha k_F/T_{c0} = 200$.

momentum scales linearly with h and the slope of $Q(h)$ curves varies linearly with the spin-orbit constant. Such behavior is consistent with the presence of the Lifshitz invariant $\propto \alpha h$ in the Ginzburg-Landau free-energy density. In accordance with our qualitative arguments in Sec. IV, the resulting $Q(h)$ dependences exhibit a reentrant behavior, and $\max_h |Q(h)|$ shifts to stronger fields as the spin-orbit energy increases. Figures 5(b) and 5(c) show corresponding $\log_{10}[Q^2(h)]$ dependences and $\log_{10}$-$\log_{10}$ plots of δT_c versus Q^2 for the chosen field range $h/T_{c0} \in [-200, 200]$. According to Eqs. (22), for the GL functional (20) $\log_{10}[\delta T_c(Q)]$ should be a linear function of $\log_{10}(Q^2)$. The plots in Figs. 5(b) and 5(c) demonstrate that the shift in the critical temperature for a modulated superconducting state is, indeed, quadratic in Q for small h and deviates from quadratic dependence for rather large h values. Therefore, the results in Figs. 5(a) and 5(c) provide a microscopic justification of the phenomenological description (20) and point out the range of the exchange fields in the adjacent layer within which such a description is valid. Our numerical calculations also reveal that the considered superconducting heterostructures can possess nonreciprocal properties. In particular, for rather large spin-splitting fields h we observe the appearance of the antisymmetric component of the function $T_c(Q+q)$ with respect to q, which indicates the possibility of the superconducting diode effect in the system, namely, the in-plane anisotropy of the critical current [85–87].

Note, in conclusion, that within the parameter range considered in our work the shift in critical temperature due to a modulated superconducting state is rather small $\delta T_c/T_{c0} < 10^{-3}$. In this regard, in the presence of the exchange field and the spin-orbit interaction nonreciprocal superconducting properties should manifest themselves within the low-temperature regime, which is beyond the scope of the present work. Nevertheless, our calculations suggest that for the enhancement of nonreciprocal effects the following conditions should be satisfied. First, the ferromagnetic layer should feature a large difference in the spin-resolved densities of states at the Fermi level. This is a typical situation in superconductor/half-metal systems. Second, an optimal value of the spin-orbit energy $\alpha k_F \sim h$ is required.

Fig. 5: $\mu_s/T_{c0} = 10^3$, $\mu_f/T_{c0} = -120$, $d_s T_{c0}/v_F = 0.05$, and $d_f = 4d_s$. We can see from Fig. 5(a) that for small h the pair

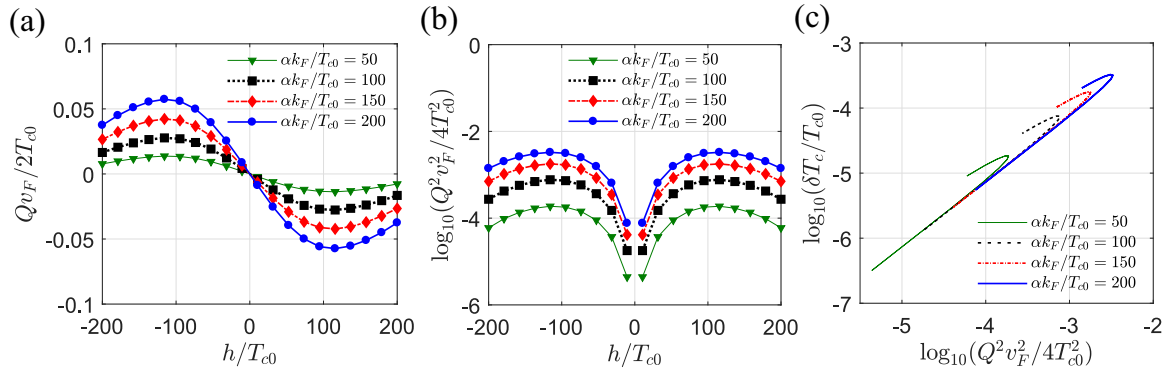

FIG. 5. (a) and (b) The dependences of the pair momentum Q and $\log_{10}(Q^2)$ on the spin-splitting field h in the adjacent layer for several spin-orbit energies, $\alpha k_F/T_{c0} = 50, 100, 150, 200$. (c) Corresponding parametric $\log_{10}$-$\log_{10}$ plots of δT_c versus Q^2. The parameters are $\mu_s/T_{c0} = 10^3$, $\mu_f/T_{c0} = -120$, $d_s T_{c0}/v_F = 0.05$, and $d_f = 4d_s$. Here $\delta T_c(Q) \equiv T_c(Q) - T_c(0)$.

VI. SUMMARY

To sum up, we have developed a microscopic theory of the inverse proximity effect for planar hybrid structures consisting of a thin superconducting film placed in contact with a material with a strong exchange or Zeeman field and Rashba spin-orbit interaction. It has been shown that the spin-orbit interaction partially compensates the pair-breaking effect of the exchange field. This effect originates from the appearance of the intraband spin-singlet pairing correlations in the superconductor for which the depairing effect of the exchange or Zeeman field becomes weaker. It has been demonstrated that the spin-orbit interaction stabilizes modulated superconducting states which can be traced to the Lifshitz invariant in the Ginzburg-Landau free-energy density. Our results provide a microscopic justification of the GL functional with the Lifshitz invariant for a large class of superconducting hybrid systems and clarify the validity range of the corresponding phenomenological models.

ACKNOWLEDGMENTS

We thank A. A. Bespalov for stimulating discussions and A. V. Samokhvalov and I. M. Khaymovich for valuable comments. This work was supported by the Russian Science Foundation (Grant No. 20-12-00053).

[1] J. Alicea, New directions in the pursuit of Majorana fermions in solid state systems, Rep. Prog. Phys. **75**, 076501 (2012).
[2] C. W. J. Beenakker, Search for Majorana fermions in superconductors, Annu. Rev. Condens. Matter Phys. **4**, 113 (2013).
[3] R. Aguado, Majorana quasiparticles in condensed matter, Riv. Nuovo Cimento **40**, 523 (2017).
[4] R. M. Lutchyn, E. P. A. M. Bakkers, L. P. Kouwenhoven, P. Krogstrup, C. M. Marcus, and Y. Oreg, Majorana zero modes in superconductor-semiconductor heterostructures, Nat. Rev. Mater. **3**, 52 (2018).
[5] A. Haim and Y. Oreg, Time-reversal-invariant topological superconductivity in one and two dimensions, Phys. Rep. **825**, 1 (2019).
[6] Y. Oreg and F. von Oppen, Majorana zero modes in networks of Cooper-pair boxes: Topologically ordered states and topological quantum computation, Annu. Rev. Condens. Matter Phys. **11**, 397 (2020).
[7] R. Aguado and L. Kouwenhoven, Majorana qubits for topological quantum computing, Phys. Today **73**(6), 44 (2020).
[8] E. Prada, P. San-Jose, M. W. A. de Moor, A. Geresdi, E. J. H. Lee, J. Klinovaja, D. Loss, J. Nygård, R. Aguado, and L. P. Kouwenhoven, From Andreev to Majorana bound states in hybrid superconductor-semiconductor nanowires, Nat. Rev. Phys. **2**, 575 (2020).
[9] K. Flensberg, F. von Oppen, and A. Stern, Engineered platforms for topological superconductivity and Majorana zero modes, Nat. Rev. Mater. **6**, 944 (2021).
[10] K. Laubscher and J. Klinovaja, Majorana bound states in semiconducting nanostructures, J. Appl. Phys. **130**, 081101 (2021).
[11] L. Fu and C. L. Kane, Superconducting Proximity Effect and Majorana Fermions at the Surface of a Topological Insulator, Phys. Rev. Lett. **100**, 096407 (2008).
[12] T. D. Stanescu, J. D. Sau, R. M. Lutchyn, and S. Das Sarma, Proximity effect at the superconductor-topological insulator interface, Phys. Rev. B **81**, 241310(R) (2010).
[13] M.-X. Wang, C. Liu, J.-P. Xu, L. Miao, M.-Yu Yao, C. L. Gao, C. Shen, X. Ma, X. Chen, Z.-An Xu, Y. Liu, S. C. Zhang, D. Qian, J.-F. Jia, and Q.-K. Xue, The coexistence of superconductivity and topological order in the Bi_2Se_3 thin films, Science **336**, 52 (2012).
[14] S.-Y. Xu, N. Alidoust, I. Belopolski, A. Richardella, C. Liu, M. Neupane, G. Bian, S.-H. Huang, R. Sankar, C. Fang, B. Dellabetta, W. Dai, Qi. Li, M. J. Gilbert, F. Chou, N. Samarth, and M. Z. Hasan, Momentum-space imaging of Cooper pairing in a half-Dirac-gas topological superconductor, Nat. Phys. **10**, 943 (2014).
[15] D. Flötotto, Y. Bai, C. Zhang, K. Okazaki, A. Tsuzuki, T. Hashimoto, J. N. Eckstein, S. Shin, and T.-C. Chiang, Superconducting pairing of topological surface states in bismuth selenide films on niobium, Sci. Adv. **4**, eaar7214 (2018).
[16] R. M. Lutchyn, J. D. Sau, and S. Das Sarma, Majorana Fermions and a Topological Phase Transition in Semiconductor-Superconductor Heterostructures, Phys. Rev. Lett. **105**, 077001 (2010).
[17] Y. Oreg, G. Refael, and F. von Oppen, Helical Liquids and Majorana Bound States in Quantum Wires, Phys. Rev. Lett. **105**, 177002 (2010).
[18] T. D. Stanescu, R. M. Lutchyn, and S. Das Sarma, Majorana fermions in semiconductor nanowires, Phys. Rev. B **84**, 144522 (2011).
[19] V. Mourik, K. Zuo, S. M. Frolov, S. R. Plissard, E. P. A. M. Bakkers, and L. P. Kouwenhoven, Signatures of Majorana fermions in hybrid superconductor-semiconductor nanowire devices, Science **336**, 1003 (2012).
[20] A. Das, Y. Ronen, Y. Most, Y. Oreg, M. Heiblum, and H. Shtrikman, Zero-bias peaks and splitting in Al-InAs nanowire topological superconductor as a signature of Majorana fermions, Nat. Phys. **8**, 887 (2012).
[21] W. Chang, S. M. Albrecht, T. S. Jespersen, F. Kuemmeth, P. Krogstrup, J. Nygård, and C. M. Marcus, Hard gap in epitaxial semiconductor-superconductor nanowires, Nat. Nanotechnol. **10**, 232 (2015).
[22] S. M. Albrecht, A. P. Higginbotham, M. Madsen, F. Kuemmeth, T. S. Jespersen, J. Nygård, P. Krogstrup, and C. M. Marcus, Exponential protection of zero modes in Majorana islands, Nature (London) **531**, 206 (2016).
[23] M. Eschrig, Spin-polarized supercurrents for spintronics, Phys. Today **64**(1), 43 (2011).
[24] J. Linder and J. W. A. Robinson, Superconducting spintronics, Nat. Phys. **11**, 307 (2015).
[25] A. Buzdin, Direct Coupling Between Magnetism and Superconducting Current in the Josephson φ_0 Junction, Phys. Rev. Lett. **101**, 107005 (2008).
[26] I. Margaris, V. Paltoglou, and N. Flytzanis, Zero phase difference supercurrent in ferromagnetic Josephson junctions, J. Phys.: Condens. Matter **22**, 445701 (2010).

[27] T. Yokoyama, M. Eto, and Yu. V. Nazarov, Anomalous Josephson effect induced by spin-orbit interaction and Zeeman effect in semiconductor nanowires, Phys. Rev. B **89**, 195407 (2014).
[28] F. Dolcini, M. Houzet, and J. S. Meyer, Topological Josephson ϕ_0 junctions, Phys. Rev. B **92**, 035428 (2015).
[29] F. Konschelle, I. V. Tokatly, and F. S. Bergeret, Theory of the spin-galvanic effect and the anomalous phase shift φ_0 in superconductors and Josephson junctions with intrinsic spin-orbit coupling, Phys. Rev. B **92**, 125443 (2015).
[30] C. Spånslätt, Geometric Josephson effects in Majorana nanowires, Phys. Rev. B **98**, 054508 (2018).
[31] S. Pal and C. Benjamin, Quantized Josephson phase battery, Europhys. Lett. **126**, 57002 (2019).
[32] A. G. Kutlin and A. S. Mel'nikov, Geometry-dependent effects in Majorana nanowires, Phys. Rev. B **101**, 045418 (2020).
[33] A. A. Kopasov, A. G. Kutlin, and A. S. Mel'nikov, Geometry controlled superconducting diode and anomalous Josephson effect triggered by the topological phase transition in curved proximitized nanowires, Phys. Rev. B **103**, 144520 (2021).
[34] D. B. Szombati, S. Nadj-Perge, D. Car, S. R. Plissard, E. P. A. M. Bakkers, and L. P. Kouwenhoven, Josephson φ_0-junction in nanowire quantum dots, Nat. Phys. **12**, 568 (2016).
[35] W. Mayer, M. C. Dartiailh, J. Yuan, K. S. Wickramasinghe, E. Rossi, and J. Shabani, Gate controlled anomalous phase shift in Al/InAs Josephson junctions, Nat. Commun. **11**, 212 (2020).
[36] E. Strambini, A. Iorio, O. Durante, R. Citro, C. Sanz-Fernández, C. Guarcello, I. V. Tokatly, A. Braggio, M. Rocci, N. Ligato, V. Zannier, L. Sorba, F. S. Bergeret, and F. Giazotto, A Josephson phase battery, Nat. Nanotechnol. **15**, 656 (2020).
[37] S. S. Pershoguba, K. Björnson, A. M. Black-Schaffer, and A. V. Balatsky, Currents Induced by Magnetic Impurities in Superconductors with Spin-Orbit Coupling, Phys. Rev. Lett. **115**, 116602 (2015).
[38] S. Mironov and A. Buzdin, Spontaneous Currents in Superconducting Systems with Strong Spin-Orbit Coupling, Phys. Rev. Lett. **118**, 077001 (2017).
[39] J. W. A. Robinson, A. V. Samokhvalov, and A. I. Buzdin, Chirality-controlled spontaneous currents in spin-orbit coupled superconducting rings, Phys. Rev. B **99**, 180501(R) (2019).
[40] A. V. Samokhvalov, A. A. Kopasov, A. G. Kutlin, S. V. Mironov, A. I. Buzdin, and A. S. Mel'nikov, Spontaneous Currents and Topologically Protected States in Superconducting Hybrid Structures with the Spin-Orbit Coupling (Brief Review), JETP Lett. **113**, 34 (2021).
[41] Zh. Devizorova, A. V. Putilov, I. Chaykin, S. Mironov, and A. I. Buzdin, Phase transitions in superconductor/ferromagnet bilayer driven by spontaneous supercurrents, Phys. Rev. B **103**, 064504 (2021).
[42] F. Ando, Y. Miyasaka, T. Li, J. Ishizuka, T. Arakawa, Y. Shiota, T. Moriyama, Y. Yanase, and T. Ono, Observation of superconducting diode effect, Nature (London) **584**, 373 (2020).
[43] W. L. McMillan, Tunneling model of the superconducting proximity effect, Phys. Rev. **175**, 537 (1968).
[44] T. Tokuyasu, J. A. Sauls, and D. Rainer, Proximity effect of a ferromagnetic insulator in contact with a superconductor, Phys. Rev. B **38**, 8823 (1988).
[45] P. Virtanen, A. Vargunin, and M. Silaev, Quasiclassical free energy of superconductors: Disorder-driven first-order phase transition in superconductor/ferromagnetic-insulator bilayers, Phys. Rev. B **101**, 094507 (2020).
[46] V. O. Yagovtsev, N. A. Gusev, N. G. Pugach, and M. Eschrig, The inverse proximity effect in strong ferromagnet-superconductor structures, Supercond. Sci. Technol. **34**, 025003 (2021).
[47] A. Hijano, S. Ilić, M. Rouco, C. González-Orellana, M. Ilyn, C. Rogero, P. Virtanen, T. T. Heikkilä, S. Khorshidian, M. Spies, N. Ligato, F. Giazotto, E. Strambini, and F. S. Bergeret, Coexistence of superconductivity and spin-splitting fields in superconductor/ferromagnetic insulator bilayers of arbitrary thickness, Phys. Rev. Research **3**, 023131 (2021).
[48] S. Vaitiekėnas, Y. Liu, P. Krogstrup, and C. M. Marcus, Zero-bias peaks at zero magnetic field in ferromagnetic hybrid nanowires, Nat. Phys. **17**, 43 (2021).
[49] V. Barzykin and L. Gor'kov, Inhomogeneous Stipe Phase Revisited for Surface Superconductivity, Phys. Rev. Lett. **89**, 227002 (2002).
[50] G. Zwicknagl, S. Jahns, and P. Fulde, Critical magnetic field of ultra-thin superconducting films and interfaces, J. Phys. Soc. Jpn. **86**, 083701 (2017).
[51] L. A. B. Olde Olthof, J. R. Weggemans, G. Kimbell, J. W. A. Robinson, and X. Montiel, Tunable critical field in Rashba superconductor thin films, Phys. Rev. B **103**, L020504 (2021).
[52] M. J. Park, J. Yang, Y. Kim, and M. J. Gilbert, Fulde-Ferrell states in inverse proximity-coupled magnetically doped topological heterostructures, Phys. Rev. B **96**, 064518 (2017).
[53] A. A. Kopasov, I. M. Khaymovich, and A. S. Mel'nikov, Inverse proximity effect in semiconductor Majorana nanowires, Beilstein J. Nanotechnol. **9**, 1184 (2018).
[54] H. C. Hugdal, M. Amundsen, J. Linder, and A. Sudbø, Inverse proximity effect in s-wave and d-wave superconductors coupled to topological insulators, Phys. Rev. B **99**, 094505 (2019).
[55] J. Baumard, J. Cayssol, A. Buzdin, and F. S. Bergeret, Interplay between superconductivity and spin-dependent fields in nanowire-based systems, Phys. Rev. B **101**, 184512 (2020).
[56] N. Sedlmayr and A. Levchenko, Hybridization mechanism of the dual proximity effect in superconductor-topological insulator interfaces, Solid State Commun. **327**, 114221 (2021).
[57] J. Delaforce, M. Sistani, R. B. G. Kramer, M. A. Luong, N. Roch, W. M. Weber, M. I. den Hertog, E. Robin, C. Naud, A. Lugstein, and O. Buisson, Al-Ge-Al nanowire heterostructure: From single-hole quantum dot to Josephson effect, Adv. Mater. **33**, 2101989 (2021).
[58] T. Shoman, A. Takayama, T. Sato, T. Takahashi, T. Oguchi, K. Segawa, and Y. Ando, Topological proximity effect in a topological insulator hybrid, Nat. Commun. **6**, 6547 (2015).
[59] C. X. Trang, N. Shimamura, K. Makayama, S. Souma, K. Sugawara, I. Watanabe, K. Yamauchi, T. Oguchi, K. Segawa, T. Takahashi, Y. Ando, and T. Sato, Conversion of a conventional superconductor into a topological superconductor by topological proximity effect, Nat. Commun. **11**, 159 (2020).
[60] V. M. Edelstein, Characteristics of the Cooper pairing in two-dimensional noncentrosymmetric electron systems, Zh. Eksp. Teor. Fiz. **95**, 2151 (1989) [Sov. Phys. JETP **68**, 1244 (1989)].
[61] V. M. Edelstein, The Ginzburg-Landau equation for superconductors of polar symmetry, J. Phys.: Condens. Matter **8**, 339 (1996).

[62] K. V. Samokhin, Magnetic properties of superconductors with strong spin-orbit coupling, Phys. Rev. B **70**, 104521 (2004).

[63] R. P. Kaur, D. F. Agterberg, and M. Sigrist, Helical Vortex Phase in the Noncentrosymmetric $CePt_3Si$, Phys. Rev. Lett. **94**, 137002 (2005).

[64] O. Dimitrova and M. V. Feigel'man, Theory of a two-dimensional superconductor with broken inversion symmetry, Phys. Rev. B **76**, 014522 (2007).

[65] V. P. Mineev and K. V. Samokhin, Nonuniform states in noncentrosymmetric superconductors: Derivation of Lifshitz invariants from microscopic theory, Phys. Rev. B **78**, 144503 (2008).

[66] M. Houzet and J. Meyer, Quasiclassical theory of disordered Rashba superconductors, Phys. Rev. B **92**, 014509 (2015).

[67] K. M. D. Hals, Magnetoelectric coupling in superconductor-helimagnet heterostructures, Phys. Rev. B **95**, 134504 (2017).

[68] W. E. Pickett and J. S. Moodera, Half metallic magnets, Phys. Today **54**(5), 39 (2001).

[69] J. M. D. Coey and M. Venkatesan, Half-metallic ferromagnetism: Example of CrO_2 (invited), J. Appl. Phys. **91**, 8345 (2002).

[70] R. S. Keizer, S. T. B. Goennenwein, T. M. Klapwijk, G. Miao, G. Xiao, and A. Gupta, A spin triplet supercurrent through the half-metallic ferromagnet CrO_2, Nature (London) **439**, 825 (2006).

[71] C. Visani, Z. Sefrioui, J. Tornos, C. Leon, J. Briatico, M. Bibes, A. Barthélémy, J. Santamaría, and J. E. Villegas, Equal-spin Andreev reflection and long-range coherent transport in high-temperature superconductor/half-metallic ferromagnet junctions, Nat. Phys. **8**, 539 (2012).

[72] A. Singh, S. Voltan, K. Lahabi, and J. Aarts, Colossal Proximity Effect in a Superconducting Triplet Spin Valve Based on the Half-Metallic Ferromagnet CrO_2, Phys. Rev. X **5**, 021019 (2015).

[73] A. A. Kamashev and I. A. Garifullin, Proximity Effect in Heterostructures Based on a Superconductor/Half-Metal System, JETP Lett. **113**, 194 (2021).

[74] S. H. Jacobsen, J. A. Ouassou, and J. Linder, Critical temperature and tunneling spectroscopy of superconductor-ferromagnet hybrids with intrinsic Rashba-Dresselhaus spin-orbit coupling, Phys. Rev. B **92**, 024510 (2015).

[75] H. T. Simensen and J. Linder, Tunable superconducting critical temperature in ballistic hybrid structures with strong spin-orbit coupling, Phys. Rev. B **97**, 054518 (2018).

[76] T. Karabassov, I. V. Bobkova, A. A. Golubov, and A. S. Vasenko, Hybrid helical state and superconducting diode effect in S/F/TI heterostructures, arXiv:2203.15608.

[77] J. M. Blatt and C. J. Thompson, Shape Resonances in Superconducting Thin Films, Phys. Rev. Lett. **10**, 332 (1963).

[78] A. A. Shanenko, M. D. Croitoru, and F. M. Peeters, Oscillations of the superconducting temperature induced by quantum well states in thin metallic films: Numerical solution of the Bogoliubov–de Gennes equations, Phys. Rev. B **75**, 014519 (2007).

[79] Y. Guo, Y.-F. Zhang, X.-Y. Bao, T.-Z. Han, Z. Tang, L.-X. Zhang, W.-G. Zhu, E. G. Wang, Q. Niu, Z. Q. Qui, J.-F. Jia, Z.-X. Zhao, and Q.-K. Xue, Superconductivity modulated by quantum size effects, Science **306**, 1915 (2004).

[80] Note that the considered spin-dependent interactions in the adjacent layer result in the change in the spin and spatial structure of the Cooper pairs in the system (see, e.g., Refs. [88,89]). However, such an analysis is not the subject of the present paper.

[81] See Supplemental Material at http://link.aps.org/supplemental/10.1103/PhysRevB.105.214508, which contains Ref. [90], for the definition of the Matsubara Green's functions, the derivation of the linearized self-consistency equation, and a detailed comparison between our numerical simulations for system configurations $\mathbf{n}_h || \mathbf{n}$ and $\mathbf{n}_h \perp \mathbf{n}$.

[82] J. Baumard, J. Cayssol, and A. Buzdin, Nonuniform superconductivity in wires with strong spin-orbit coupling, Eur. Phys. J. B **93**, 130 (2020).

[83] M. Smidman, M. B. Salamon, H. Q. Yuan, and D. F. Agterberg, Superconductivity and spin-orbit coupling in noncentrosymmetric materials: A review, Rep. Prog. Phys. **80**, 036501 (2017).

[84] G. P. Mazur, N. van Loo, J. Y. Wang, T. Dvir, G. Wang, A. Khindanov, S. Korneychuk, F. Borsoi, R. C. Dekker, G. Badawy, P. Vinke, S. Gazibegovic, E. P. A. M. Bakkers, M. Quintero-Peréz, S. Heedt, and L. P. Kouwenhoven, Spin-mixing enhanced proximity effect in aluminum-based superconductor-semiconductor hybrids, arXiv:2202.10230.

[85] N. F. Q. Yuan and L. Fu, Supercurrent diode effect and finite momentum superconductivity, PANS **119**, e2119548119 (2022).

[86] J. J. He, Y. Tanaka, and N. Nagaosa, A phenomenological theory of superconductor diodes, New J. Phys. **24**, 053014 (2022).

[87] A. Daido, Y. Ikeda, and Y. Yanase, Intrinsic Superconducting Diode Effect, Phys. Rev. Lett. **128**, 037001 (2022).

[88] V. M. Edelstein, Triplet superconductivity and magnetoelectric effect near the *s*-wave-superconductor-normal-metal interface caused by local breaking of mirror symmetry, Phys. Rev. B **67**, 020505(R) (2003).

[89] C. R. Reeg and D. L. Maslov, Proximity-induced triplet superconductivity in Rashba materials, Phys. Rev. B **92**, 134512 (2015).

[90] N. Kopnin, *Theory of Nonequilibrium Superconductivity* (Oxford University Press, Oxford, 2001).